ORIGINAL RESEARCH ARTICLE

Understanding of the Microstructure Evolution and Wear Resistance of Cr12MoV Die Steel during Deep Cryogenic Treatment

Caidong Zhang, Jie Li, Yunfei Zhang, Zhiyan Sun, Shuai Ren, Da Lv, Baoguo Nian, Yingli Zhao, and Yue Song

The present study investigated the influence of deep cryogenic treatment (DCT) on the microstructure evolution and wear resistance of Cr12MoV die steel. Four types of heat treatments (quenching + tempering (QT), quenching + DCT (QC), quenching + DCT + tempering (QCT) and quenching + tempering + DCT (QTC)) were utilized to obtain different microstructure and mechanical properties. The hardness, impact toughness, weight loss, frictional coefficient, volume fraction of retained austenite (RA), secondary nanometric carbides (SNC) and worn surface morphology were investigated in detail to discuss the relation between microstructure evolution and wear mechanism changes induced by DCT. The results show that the precipitation of SNC has less effect on hardness than the decrease of carbon content in martensite that caused by DCT and tempering. The principal reason for the high hardness and low toughness without tempering is the high carbon content in martensite. The RA volume fraction has greater effect on the hardness and toughness in condition of tempering. Four types of wear cracks (matrix cracks, boundary cracks, extension cracks and carbide cracks) were identified for the analysis of worn surface morphology. When the matrix hardness is high and RA volume fraction is relatively low, the wear cracks were mainly carbide cracks and extension cracks, accompanied by a few of boundary cracks. When the matrix hardness is low and the RA volume fraction is relatively high, the wear cracks were mainly matrix cracks, accompanied by some boundary cracks and extension cracks. DCT affects the wear mechanism of Cr12MoV die steel by facilitating the transformation of RA and the precipitation of SNC.

1. Introduction

Cr12MoV die steel is widely used in the field of mechanical manufacturing (Ref 1). In high carbon content steels, the finish temperature of martensite is below 0 °C, which means some austenite named "retained austenite" is retained after the conventional heat treatment (Ref 2). Some problems could be appeared during the service process as the RA could be transformed into martensite which is more brittle than the tempered one (Ref 3). DCT is a form of heat treatment technology (Ref 4, 5) with simple application (Ref 6), cost-effective (Ref 7) and positive effect on the reduction of RA (Ref

8-10), hardness (Ref 11-15) and wear resistance (Ref 16-18). DCT is so important for a lot of fields, such as materials science (Ref 19, 20), medicine (Ref 21), the fuel and energy sectors (Ref 22) and steel industries (Ref 23, 24). The microstructural evolution that caused by DCT is considered as: a more homogenous microstructure (Ref 25, 26), precipitation of finer carbides (Ref 27, 28), transformation of RA into martensite (Ref 29, 30), the specific orientation of newly formed martensite laths (Ref 31), formation of finer martensite laths (Ref 32), various oxidation dynamics (Ref 33) and chemical shifts of alloying elements on the surface (Ref 27). However, despite extensive researches conducted by lots of scholars in the past few years, the mechanisms for the powerful impact by DCT, especially the significant improvement in wear resistance, are still not fully understood.

Some theories were proposed to explain the effect of DCT on microstructure and mechanical properties. The most popular theory claims that the structure contraction that caused by the low temperature induces the precipitation of small secondary carbides. Due to the contraction coefficients of martensite and RA are different, the carbon atoms would jump to the adjacent dislocations under the state of high contraction and act as a nucleation site for the future carbide during tempering (Ref 34). A newer theory claims that the transformation of RA is caused by the plastic deformation of original martensite. The plastic deformation leads to dislocations that can capture immovable carbon atoms, forming carbon clusters that serve as nucleation points during subsequent tempering processes to form carbides (Ref 35, 36). Another theory was postulated by some

Caidong Zhang, Jie Li, Zhiyan Sun, Shuai Ren, Da Lv, Baoguo Nian, Yingli Zhao, and Yue Song, HBIS Materials Technology Research Institute, HBIS Group, Shijiazhuang 050000, People's Republic of China; and Yunfei Zhang, HBIS Materials Technology Research Institute, HBIS Group, Shijiazhuang 050000, People's Republic of China; and Key Laboratory of Ultralight Materials and Surface Technology of Ministry of Education, School of Materials Science and Chemical Engineering, Harbin Engineering University, Harbin 150001, People's Republic of China. Contact e-mails: zhangcaidong@hbisco.com, sunzhiyan@hbisco.com, and renshuai@hbisco.com.

researchers (Ref 26, 37) that DCT improves the driving force of carbide nucleation by reducing the lattice energy and promoting the transformation of RA to form finer martensite, which jointly leads to the finer carbides and increased precipitation. On the contrary, Gavriljuk et al. (Ref 38) considered that the nucleation of carbide occurs as the direct plastic deformation of martensite during DCT. Antony et al. (Ref 39) explained that the supersaturation of martensite improves the thermodynamic instability and lattice distortion during DCT, which facilitates the migration of alloying and carbon atoms toward adjacent crystal defects.

As outlined above, researches about DCT mainly concentrated on the microstructure changes correspondence with mechanical properties. The changes in wear mechanism caused by DCT are not fully understood yet. Changing the duration time of DCT or the sequence of DCT and tempering is an effective method to obtain different microstructures and wear resistance (Ref 40-45). For the first time, four different heat treatments (QT, QC, QCT, and QTC) were used to obtain various microstructure and mechanical properties of Cr12MoV die steel in this work. The microstructure and worn surface morphology was investigated in detail by Zeiss Lsm700 laser scanning confocal microscope (LSCM) and Zeiss Ultra 55 scanning electron microscopes (SEM) to discuss the relation between wear mechanism changes and the microstructure evolution caused by DCT. Our findings reveal the wear failure mechanism of Cr12MoV die steel under different microstructures, which provides a necessary understanding for the efficient using of DCT on tool steels.

2. Experimental Procedure

The chemical composition of Cr12MoV die steel was presented in Table 1. DCT was performed by gradually cooling the samples to -196 °C and holding them at that temperature for 6h, then "air heating" to room temperature. The sequences and characteristics of the applied treatments were shown in Table 2.

The hardness, impact toughness and wear resistance tests were measured at room temperature. The samples for optical metallography (OM) observation were polished up to 1000 mesh and etching with 4% nital. The Brinell hardness (HB) was tested by Wilson BH3000 hardness tester at the scale of HBW10/3000. Five points were tested for each sample to get the average value. Zwick/Roell 450 J impact tester was used to measure the impact toughness. The size of the impact specimen was $10 \times 10 \times 55$ mm with a V-notch and tested at room temperature. Three parallel samples were measured and the mean values were taken as the impact absorption energy. The contents of the RA were tested by PANalytical Empyrean x-ray diffraction instrument. The relative proportion of martensite and austenite was calculated by the equation provided in Ref. (Ref 46). The effect of DCT on friction and wear resistance was studied by UMT TriboLab friction and wear tester. The parameter settings of friction and wear test were listed in Table 3. LSCM and SEM were utilized to characterize the worn surface morphology. The elemental contents of various phases were measured by the energy dispersive x-ray spectroscopy (EDS) system of SEM.

3. Results and Discussion

3.1 Microstructure Evaluation

Figure 1 depicts the OM maps of HT1-4 samples subjected to different heat treatment sequences. It is obvious that three phases (martensite, RA and carbides) are presented in the samples, as described by Yildiz (Ref 47). The implementation of DCT had a noticeable influence on the microstructure, promoting the transformation of RA into martensite. Figure 2 shows the x-ray diffraction of HT1-4 samples. The volume fraction of RA was estimated based on ASTM standard, taking into account the diffraction crystal planes (1 1 1), (2 0 0), (2 2 0) of austenite and (0 1 1), (0 0 2), (1 1 2) of martensite (Ref 48). The results of the measured RA volume fraction were listed in Table 4. Any form of DCT reduces the RA volume fraction of Cr12MoV die steel. These results are consistent with previous studies, as the decrease of RA volume fraction typically reported when applying DCT (Ref 35, 49-52). It was found that tempering was a good method for the transformation of RA into martensite after DCT by comparing the results of HT2 and HT3. The type of QCT leads to the least RA volume fraction (2%) in this study. The method of DCT has an obvious effect on the RA volume fraction. For HT2 and HT3 samples, which were subjected to cryogenic treatment directly after quenched, a higher volume of retained austenite (RA) was observed in comparison to HT4 sample which was tempered first. This phenomenon is due to the stabilization of austenite during the tempering process (Ref 53). Austenite stabilization reduces the volume fraction of RA that can be transformed by DCT. These remaining RA still cannot be fully transformed, even after second tempering. It indicates that Cr12MoV die steel has a minimum inherent RA content, which cannot be converted through traditional heat treatment. This is consistent with the viewpoint of Li et al. (Ref 52) who also expressed the inherent RA content after tempered. Cryogenic treatment not only promotes the reduction of RA (Ref 54) and the increase of martensite, but also increases the amounts of fine secondary carbides. As mentioned above, microstructure of HT1-4 samples consists of martensite, RA, and carbides, shown as Fig. 1. The x-ray diffraction patterns (Fig. 2) show that the carbides present in matrix are M_7C_3. The EDS analysis of carbides and the matrix is illustrated in Fig. 3. The results suggest that the identified carbides are chromium carbides. There are three kinds of chromium carbides with different morphologies: quite large primary carbides (red circle), secondary micrometric carbides (green circle) and SNC (blue

**Table 1 Chemical compositions of the Cr12MoV die steel used in this study**

Elements	C	Si	Mn	Cr	Mo	V	P	S	Fe
wt, %	1.51	0.28	0.37	12.0	0.53	0.29	0.008	0.005	Bal.

Table 2 Heat treatment sequences of Cr12MoV die steel used in this study

Sample	Processing sequences		
HT1	Austenitizing at 1030 °C for 20min, followed by air quench	Tempering at 200 °C for 2h	
HT2	Austenitizing at 1030 °C for 20min, followed by air quench	DCT at − 196 °C for 6h	
HT3	Austenitizing at 1030 °C for 20min, followed by air quench	DCT at − 196 °C for 6h	Tempering at 200 °C for 2h
HT4	Austenitizing at 1030 °C for 20min, followed by air quench	Tempering at 200 °C for 2h	DCT at − 196 °C for 6h

Table 3 Parameter settings of the friction and wear experiment in this study

Test standard	Test form	Friction pair material	Friction pair size	Friction velocity	Friction frequency	Test time	Test Temperature
ASTM G133-02	Reciprocating	Si_3N_4	9.525mm	24 mm/s	3Hz	3600s	26 °C
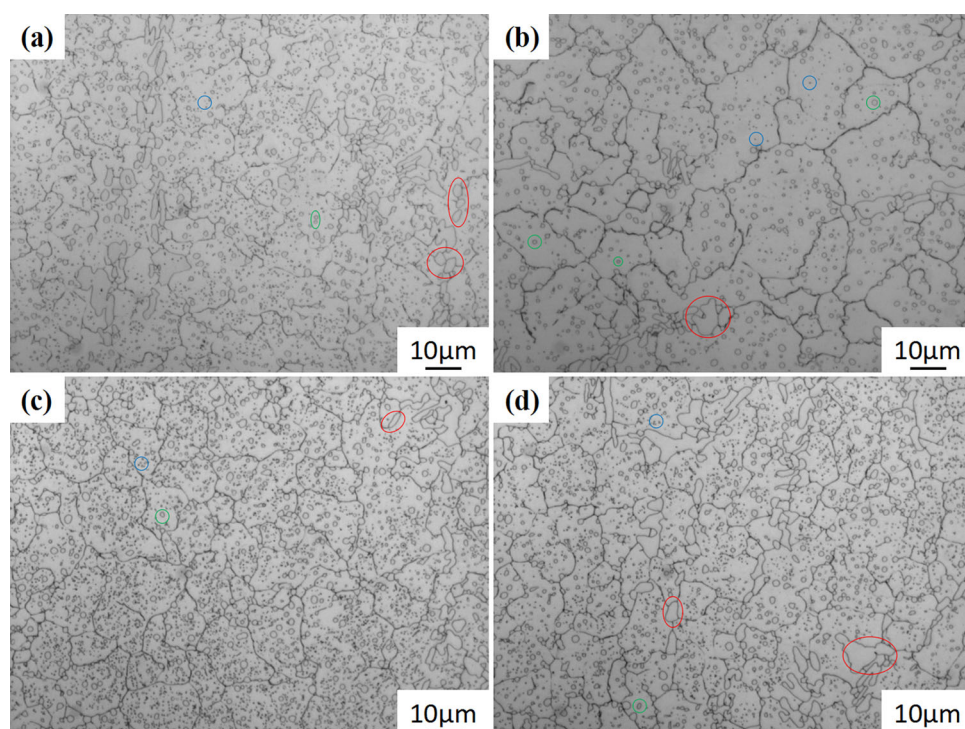
Fig. 1 OM maps of the Cr12MoV die steel after different heat treatment: (a) HT1 sample (b) HT2 sample (c) HT3 sample (d) HT4 sample

circle) distributed in the matrix of the HT1-4 samples (Fig. 1). Figure 4 shows the EBSD maps of the HT2 samples. Two types of carbides (Cr_7C_3 and $Cr_{23}C_6$) were existed in the matrix. Compared with Fig. 1, it is obvious that the type of quite large primary carbides and secondary micrometric carbides is Cr_7C_3. The type of the SNC is $Cr_{23}C_6$. The amount and volume fraction of the SNC in HT3 (Fig. 1c) and HT4 (Fig. 1d) samples increased significantly compared with HT1 (Fig. 1a) samples. In addition, the HT3 (Fig. 1c) and HT4 (Fig. 1d) samples show a more uniform distribution of the SNC than HT1 (Fig. 1a) sample. The results are consistent with previous studies (Ref 10, 55) about the influence of DCT on SNC: DCT leads to a finer, homogeneous and intensive carbide network. Furthermore, compared with HT4 (Fig. 1d) samples, the HT3 (Fig. 1c)

samples have a higher number of SNC and a more uniform distribution. However, the volume fraction of the SNC in HT2 (Fig. 1b) samples is less than HT1 (Fig. 1a) samples. The morphology and particle size of the large primary carbides and the secondary micrometric carbides in the HT1-4 samples are very similar. This is related to the forming mechanism of carbides. The primary carbides are precipitated from the liquid phase during the solidification process. The morphology and volume fraction of primary carbides remain largely unaffected by subsequent quenching and heat treatment. The secondary micrometric carbides are precipitated from matrix during quenching and cooling. Their morphology and volume fraction are almost only affected by quenching temperature and cooling rate. Therefore, the morphology and volume fraction of the
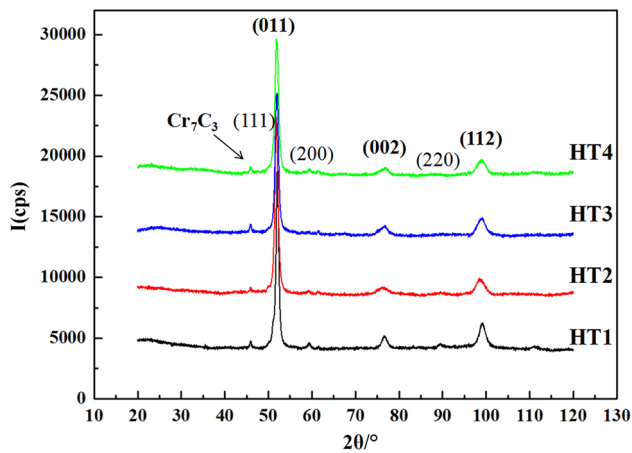
Fig. 2 The x-ray diffraction of the HT1-4 samples after different heat treatment

Table 4 The volume fraction of RA, hardness and impact toughness of the test steel

Sample	RA volume fraction, %	Hardness, HBW	Impact toughness, J
HT1	13	677	4.8
HT2	7	773	2.4
HT3	2	712	3.9
HT4	9	688	4.1

primary and secondary micrometric carbides of HT1-4 samples are almost the same.

The precipitation of SNC is influenced by the tempering and DCT processes. Martensite is a supersaturation solid solution of carbon atoms in α-Fe. Carbon atoms bear great compressive stress in the lattice. During the quenching process, due to the thermal stress and the transformation of austenite to martensite, a strong internal stress state is generated. The thermal stresses cause a great amount of structural defects and make carbon supersaturated martensite unstable. Under the thermal stresses, carbon atoms move toward structural defects through two mechanisms to form clusters: short-range diffusion mechanism (Ref 56, 57), or moving with dislocations that capture and transport carbon atoms (Ref 35). In any case, martensite decomposition and SNC precipitation occurs during tempering (Ref 58, 59). Thus, an obvious precipitation of SNC arose on the multitudinous defects during the first tempering stage, as shown in Fig. 1a. Compared with HT1 samples, HT2 samples was subjected to DCT directly after quenching, resulting in martensite lattice contraction. The lattice shrinkage of martensite at cryogenic temperatures was along with plastic deformation, which captures stationary carbon atoms by the movement of dislocations (Ref 35). During the DCT, the forced diffusion of carbon atoms, contributing to the formation of new carbide clusters, could provide nucleation sites for SNC during the warming up process.

New carbide clusters acting as nuclear sites for SNC during the warming up process were formed by the the forced diffusion of carbon atoms during DCT (Ref 15). As mentioned before, DCT can decrease the RA volume fraction of Cr12MoV die steel. The transformation of RA to martensite during DCT

causes additional compressive stress in the lattice, which can act as a carbide nucleus. Therefore, a small amount of SNC exists in HT2 samples even without tempering, as shown in Fig. 1b. Due to the low temperature during DCT, the movement of dislocations and the diffusion of carbon atoms are difficult. That is why the number of SNC in HT2 samples is significantly less than that in tempered samples. The extra carbon clusters that induced by DCT can also serve as nuclear sites for SNC during tempering in HT3 samples, leading to the higher volume fraction of SNC compared with HT1 and HT2 samples. With the precipitation of SNC and the decomposition of martensite during tempering, the compressive stress that caused by quenching and the transformation of RA was released. When DCT was applied after tempering (HT4), the precipitation of SNC during DCT was mainly induced by the lattice contraction and the transformation of RA. Since the existence of tempering stability, there was more RA in HT4 samples, resulting in lower amount of SNC than that of HT3 samples.

3.2 Hardness and Impact Toughness

The Brinell hardness results were listed in Table 4. DCT enhanced the hardness by providing more martensite and secondary carbides, which is consistent with previous research (Ref 60). Under the traditional heat treatment conditions, the hardness of HT1 samples was 677HB. When DCT was applied instead of tempering after quenching, the hardness of HT2 samples reached 773HB, which was 14.2% higher than that of HT1 samples. In the case of QCT, the hardness of HT3 saFmples was 712HB, indicating a 7.9% reduction compared with HT2 samples, but a 5.2% increase when compared with HT1 samples. Reversing the order of DCT and tempering, the hardness of HT4 samples was 688HB, which was reduced by 3.4% when compared with HT3 samples and increased by 1.6% when compared with HT1 samples.

In addition, the DCT samples (HT2-4) of Cr12MoV die steel showed significant lower impact toughness than the traditional heat treatment samples (HT1), shown as Table 4. Under the traditional heat treatment processes, the impact toughness of HT1 samples was 4.8J. When DCT was applied instead of tempering after quenching, the impact toughness of HT2 samples decreased to 2.4J, which was reduced by 50% compared with HT1 samples. In the case of QCT, the impact toughness of HT3 samples was 3.9J, which was 1.5J higher than that of HT2 samples and 18.8% lower than that of HT1 samples. Reversing the sequence of DCT and tempering, the impact toughness of HT4 samples was 4.1J, which was increased by 0.2J compared with HT3 samples and decreased by 14.6% compared with HT1 samples. Obviously, the type of DCT has a significant effect on the enhancement in hardness and the reduction in impact toughness of Cr12MoV die steel.

The influence of DCT on hardness and impact toughness of Cr12MoV die steel is the interactive effect of martensite decomposition and the transformation of RA. Any form of DCT can lead the transformation of RA into martensite, as shown in Fig. 2 and Table 4. RA is a kind of soft phase with face-centered cubic structure, which can alleviate the structural stress and deformation stress caused by martensite transformation and improve the toughness of steel (Ref 53). Figure 4(b) shows the distribution of martensite and RA. It can be seen from Fig. 4(b) that the RA is distributed around the martensite uniformly. Since the low stacking fault energy of RA, the shrinkage of lattice caused by rapid cooling and the structural
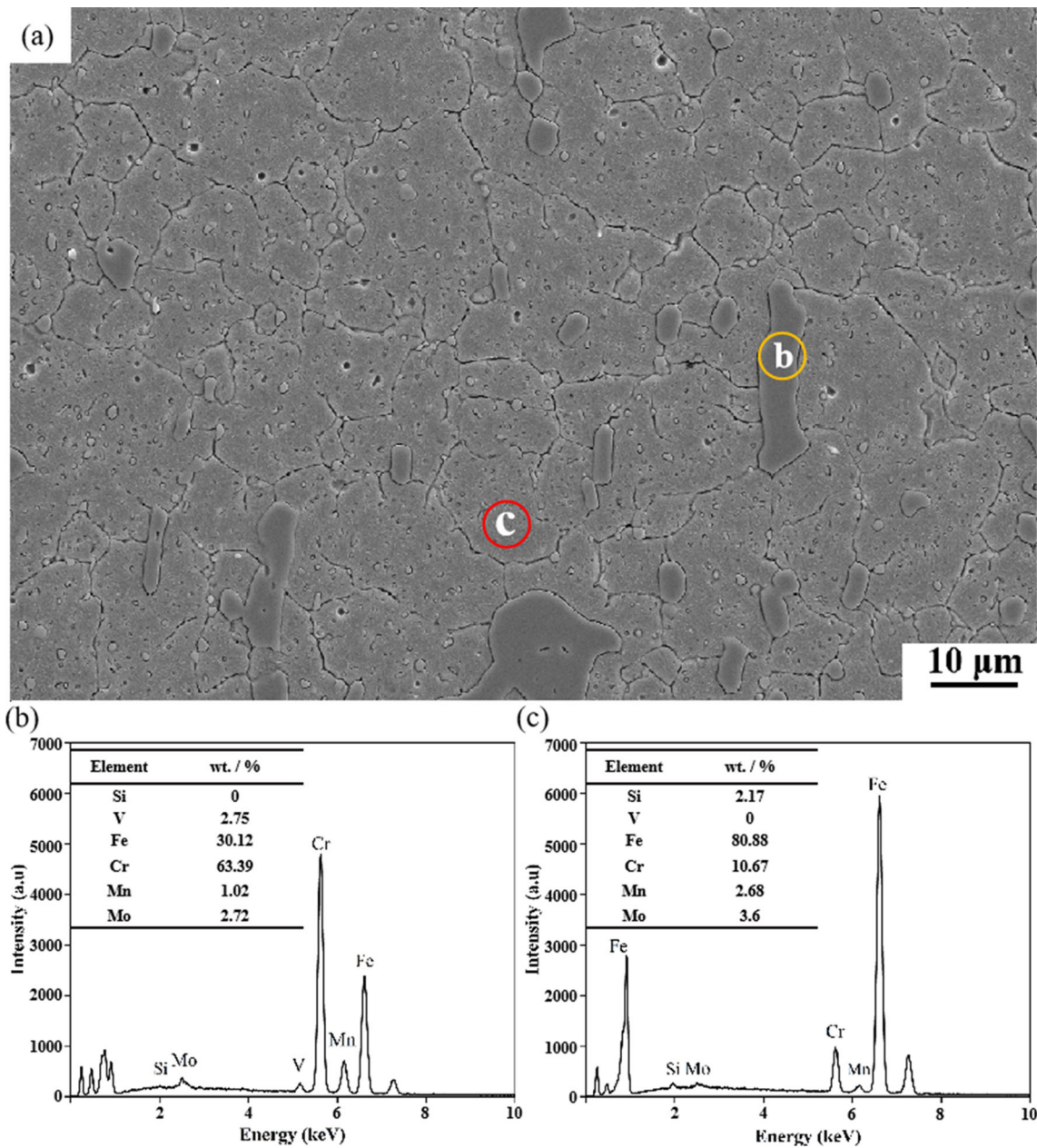
Fig. 3 SEM image and EDS analysis of HT3 sample: (a) SEM image (b) EDS analysis of carbides (c) EDS analysis of matrix
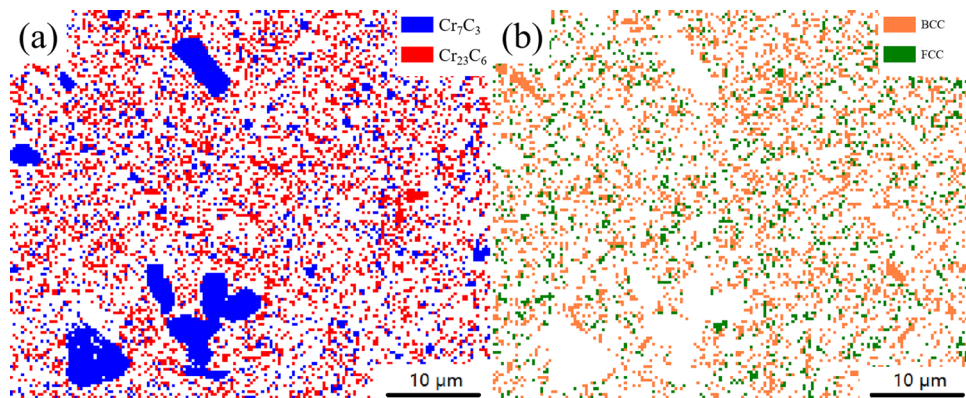

Fig. 4 EBSD maps of HT2 sample

stress and deformation stress generated by martensite transformation makes the lattice of RA slip on the stacking surface, forming micro twin substructure to release the stress. These RA with twin substructure exist around martensite in the form of broken films after DCT (Fig. 5), which can slow down the initiation and expansion of cracks. This is also one of the reasons that why HT2 samples has certain degree of impact toughness. The lattice shrinkage caused by DCT leads to the precipitation of carbon atoms from the martensitic matrix, forming SNC as depicted in Fig. 5. Consequently, this process reduces the carbon content within the martensite matrix, weakening the impact of solid solution strengthening. Therefore, DCT lead to the reduction of hardness and the enhancement of toughness from the perspective of carbon content in martensite. The SNC precipitated and dispered from martensite will interact with dislocations through the precipitate shearing mechanism and Orowan looping mechanism (Ref 61, 62) and then decrease the number of dislocations that can move to the dislocation pileup group. The SNC with high number density and uniform distribution not only play a dispersion strengthening role, but also inhibit crack initiation at the matrix-precipitation interface by relaxing the stress concentration (Ref 63, 64), thereby enhance the hardness and toughness. Therefore, DCT can strengthen the hardness and toughness simultaneously from the view of SNC. Tempering treatment also promotes the precipitation of SNC and the decomposition of martensite. The influence of tempering treatment on hardness and toughness is similar to that of DCT (Ref 65).

As the SNC are precipitated from the matrix, more SNCs suggest a lower carbon content in martensite. The amount of SNC in HT2 samples is much fewer than that in other samples (Fig. 1). Then it can be inferred that the carbon content in martensite of HT2 samples is the highest of the four samples. The hardness of HT2 samples is higher than HT3 samples, which can be analyzed from the three factors that affect the hardness of steel mentioned above. The RA volume fraction of HT2 samples (7%) is higher than HT3 samples (2%), leading to a lower hardness of HT2 samples compared with HT3 samples. The amount of SNC in HT2 samples is much lower than HT3 samples, resulting in the hardness of HT2 samples is lower than HT3 samples. The carbon content of martensite in HT2 samples is higher than HT3 samples, resulting in the hardness of HT2 samples higher than HT3 samples. Therefore, the primary reason for the higher hardness in HT2 samples compared with HT3 samples is the high carbon content in the martensite of
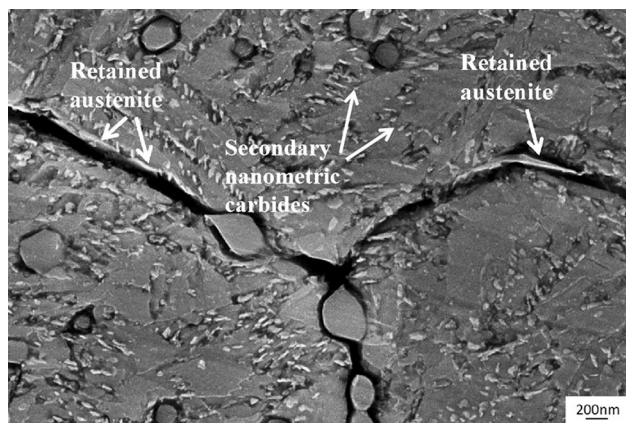
HT2 samples. At the same time, it can be inferred that the precipitation of SNC has less effect on the hardness than the reduction of carbon content in martensite. The hardness of HT3 samples is higher than HT4 samples. The RA volume fraction of HT3 samples (2%) is lower than HT4 samples (9%), resulting in the hardness of HT3 samples is higher than HT4 samples. The amount of SNC in HT3 samples is a little higher than that in HT4 samples, resulting in the hardness of HT3 samples is a little higher than HT4 samples. The carbon content in martensite of HT3 samples is a little lower than HT4 samples, resulting in the hardness of HT3 samples is a little lower than HT3 samples. Therefore, the low RA volume fraction of HT3 samples is the main reason that HT3 samples have higher hardness than HT4 samples. This is also the principal consideration that the hardness of HT4 samples is higher than HT1 samples.

The toughness of HT2 samples is lower than HT3 samples, which can also be analyzed from the three factors (RA, SNC, and the carbon content in martensite). The higher the RA content, the lesser the SNC, and the higher the carbon content in martensite. The content of RA is positively correlated with toughness. From the perspective of RA volume fraction, it is expected that the toughness of HT2 samples wolud be higher than that of HT3 samples. However, the toughness of HT2 samples is lower than HT3 samples, which may be attributed to the less SNC and the high carbon content of martensite in HT2 samples. Therefore, compared with HT4, it could be concluded that the principal consideration for the lower toughness of HT3 is the less RA volume fraction, using the same analysis method. Similarly, compared with HT1 samples, the less RA volume fraction of HT4 samples plays a main role in leading to the lower toughness.

As a summary, compared with the reduction in carbon content in martensite, SNC contributes less to the hardness value. The primary factor contributing to the high hardness and low toughness of Cr12MoV die steel in the absence of tempering is the high carbon content present in the martensite phase. The volume fraction of RA plays a more significant role in influencing the hardness and toughness of the steel during the tempering process.

3.3 Wear Resistance

The weight loss results of HT1-4 samples were listed in Table 5. It is evident that DCT significantly enhances the wear resistance. Under the traditional heat treatment conditions, the weight loss of HT1 samples was 0.0009g. When DCT was applied instead of tempering after quenching, the weight loss of HT2 samples reduced to 0.0002g, which had improvement of 77.8% weight loss than HT1 samples. As the type of QCT, the weight loss of HT3 samples was 0.0004g, which was 0.0002g more than HT2 samples and 55.6% less than HT1 samples.

Fig. 5 SEM image of HT2 sample

Table 5 The weight loss and frictional coefficient of the test steel

Sample	Weight loss, g	Average frictional coefficient
HT1	0.0009	0.83
HT2	0.0002	0.79
HT3	0.0004	0.81
HT4	0.0008	0.82

Reversing the sequence of DCT and tempering, the weight loss of HT4 samples was 0.0008g, which was 0.0004g higher than HT3 samples and only 11.1% less than HT1 samples. The lowest weight loss was achieved in the cryogenic and no tempered samples (HT2) as tempering process caused the decomposition of martensite (Ref 66).

Figure 6 shows the variation curve of the friction coefficient with sliding time of Cr12MoV die steel. The HT1 sample is denoted by the black line, HT2 by the red line, HT3 by the blue line, and HT4 by the green line. After sliding for 900s, most of the samples run to a steady-state state due to the low stick-slip effect (Ref 67). The oxide layers on contact surfaces could block the stick-slip motion at the beginning to make the frictional coefficient unstable. The oscillation in frictional coefficient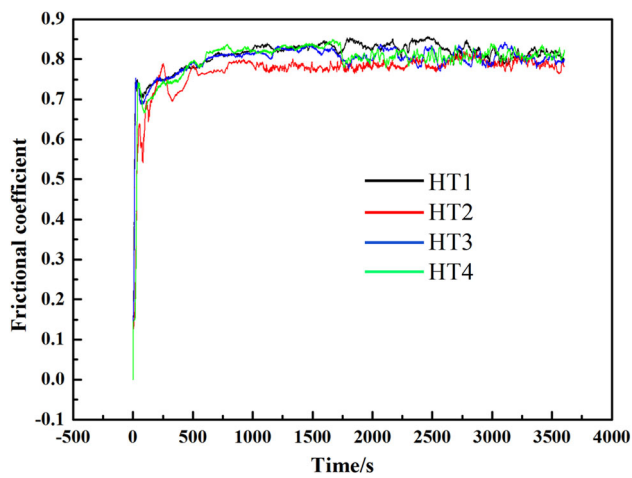 of the samples may be caused by the delimitation of thin oxide layers that cannot reach the critical thickness (Ref 68).

The average frictional coefficients of HT1-4 samples were shown in Table 5. The DCT samples (HT2-4) of Cr12MoV die steel showed significant lower average frictional coefficient than the traditional heat treatment samples (HT1). Under traditional heat treatment conditions, the average frictional coefficient of HT1 samples was 0.83. When DCT was applied instead of tempering after quenching, the average frictional coefficient of HT2 samples decreased to 0.79, which was 4.8% lower than HT1 samples. As the type of QCT, the average frictional coefficient of HT3 samples was 0.81, which was 0.02 higher than HT2 samples and 2.4% lower than HT1 samples. Reversing the sequence of DCT and tempering, the average frictional coefficient of HT4 samples was 0.82, which was 0.01 higher than HT3 samples and 1.2% lower than HT1 samples. The lowest average frictional coefficient was obtained in the HT2 samples, due to the highest hardness of the four samples (Ref 40, 69, 70). Obviously, the type of DCT has a significant influence on the average frictional coefficient of Cr12MoV die steel. According to the weight loss and frictional coefficient results, no tempering may be recommend instead of tempering treatment to obtain better wear behavior.

Figure 7 shows the SEM images of the full field worn surface of the four samples. The HT1-4 samples exhibit similar worn surface morphology, which mainly consisted of scratch lines and micro-plowing. The wear mechanisms of the four samples were micro-plowing and micro-cutting.

The worn surface morphologies of the four samples were observed by LSCM, as shown in Fig. 8. The most noticeable thing in Fig. 8 is the change of groove depths from top to bottom. The DCT samples (HT2-4) showed significant shallower grooves than the traditional heat treatment samples (HT1). Considering all tests were performed at the same condition, the reduction in the groove depths can be a symbol of better wear resistance. Under the traditional heat treatment conditions, the maximum groove depth of HT1 samples
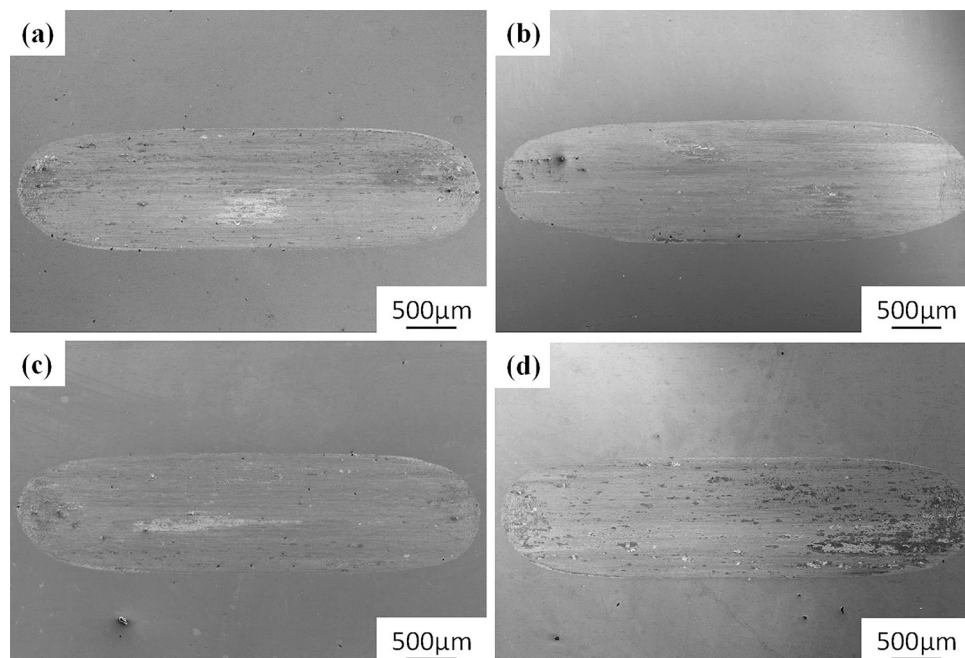

Fig. 6 The sliding time-dependent frictional coefficient curves of HT1 (black line), HT2 (red line), HT3 (blue line), and HT4 (green line) (Color figure online)

Fig. 7 SEM images of the full field worn surface of HT1-4 samples: (a) HT1 sample (b) HT2 sample (c) HT3 sample (d) HT4 sample
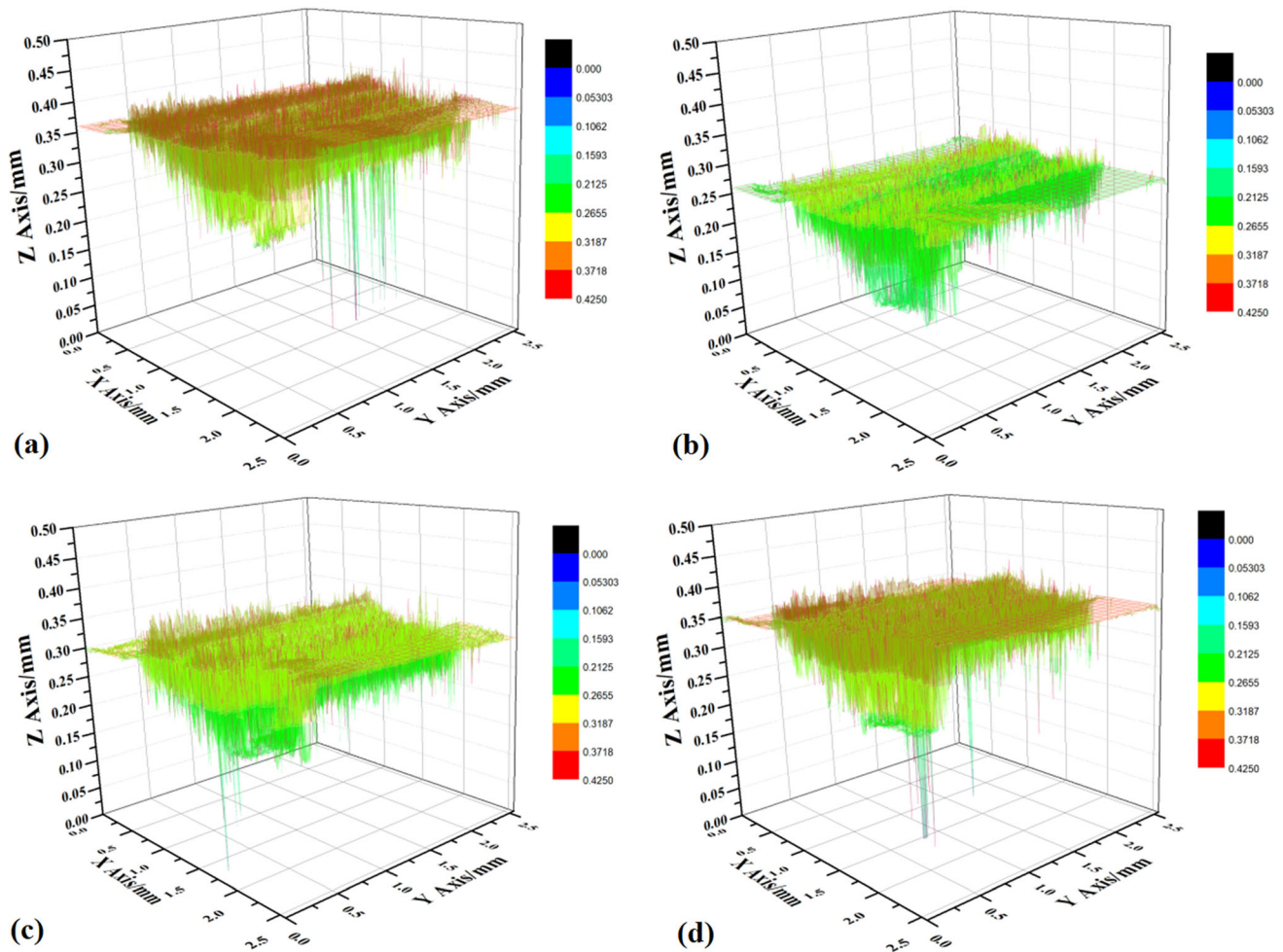
Fig. 8 LSCM images of the worn surface of HT1-4 samples: (a) HT1 sample (b) HT2 sample (c) HT3 sample (d) HT4 sample

(Fig. 8a) was 0.36mm. When DCT was applied instead of tempering after quenching, the maximum groove depth of HT2 samples (Fig. 8b) decreased to 0.26mm, which was 27.8% shallower than HT1 samples. As the type of QCT, the maximum groove depth of HT3 samples (Fig. 8c) was 0.3 mm, which was 0.04 mm deeper than HT2 samples and 16.7% shallower than HT1 samples. Reversing the sequence of DCT and tempering, the maximum groove depth of HT4 samples (Fig. 8d) was 0.35 mm, which was 0.05 mm deeper than HT3 samples and 2.8% shallower than HT1 samples. At the same time, it can be observed that the amount of large deep grooves in HT1 samples was significantly higher than that of other samples. The enhancement in wear resistance may be related to the transformation of RA into martensite, the precipitation of SNC and the change of carbon content in martensite that caused by DCT.

To better comprehend the wear mechanism, the worn surface morphologies of the HT1-4 samples were characterized by SEM with the signal of AsB, as shown in Fig. 9. It can be seen from Fig. 9 that a lot of cracks exist on the worn surface of the samples. According to the location of cracks and their relationship with carbides, these cracks can be divided into four categories that marked with yellow, green, blue, and black arrows in Fig. 9. The cracks marked with yellow arrows (matrix cracks) exist on the matrix and do not intersect with the primary carbides significantly. The cracks marked with green arrows

(boundary cracks) are located at the junction of the matrix and the primary carbides. The type of cracks marked with the blue arrows (extension cracks) is a crack where the primary carbide breaks and extends to the substrate. The type of cracks marked with the black arrows (carbide cracks) exists on the primary carbide and does not extend to the substrate.

In HT1 (Fig. 9a) and HT4 (Fig. 9d) samples, the cracks are mainly matrix cracks, accompanied by a small number of boundary cracks and extension cracks, and carbide cracks were not observed. The amount of matrix cracks in HT1 samples is higher than that in HT4 samples. The cracks are mainly extension cracks and carbide cracks, and matrix cracks or boundary cracks were note observed in HT2 samples (Fig. 9b). In HT3 samples (Fig. 9c), the cracks are mainly boundary cracks, extension cracks, and carbide cracks, and matrix cracks were not observed.

As mentioned above, the hardness (773HB) and carbon content in martensite of HT2 samples are the highest of the four samples. The number of SNC is the lowest. Therefore, it can be considered that the matrix structure of HT2 samples has the highest hardness. Higher hardness provides higher resistance to sliding contact applications, as expected from the usually effective relationship between hardness and wear resistance (Ref 40, 71, 72). At the same time, a certain amount of RA was contained in HT2 samples, leading to the relatively higher toughness than the primary carbides. Therefore, the primary
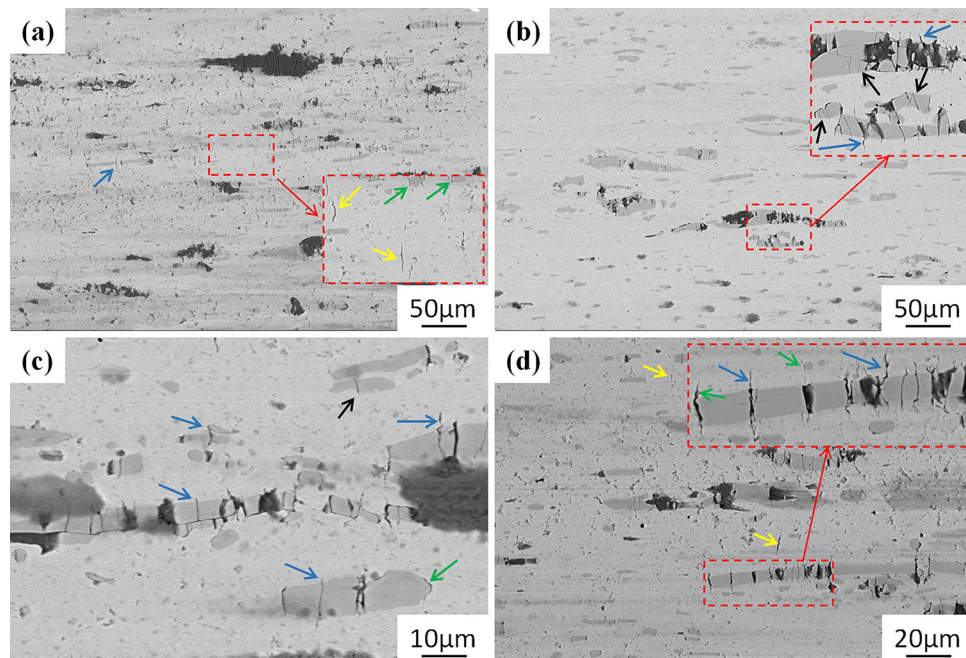
Fig. 9 SEM images of the worn surface morphology with the signal of AsB of HT1-4 samples: (a) HT1 sample (b) HT2 sample (c) HT3 sample (d) HT4 sample

carbides with almost no toughness were broken and the carbide cracks were formed. Only part of the carbide cracks can extend to the matrix to form extension cracks since the matrix strength of HT2 sample is high. Then, the cracks of HT2 samples are mainly carbide cracks and extension cracks, and the frictional coefficient and weight loss are the smallest of the four samples.

The hardness of HT3 (712HB) samples is second only to HT2 sample due to the most SNC, the least carbon content in martensite, and the minimum RA volume fraction (2%). Since the RA plays a main role in the hardness and toughness of the steel in condition of tempering mentioned above, the matrix hardness of HT3 samples is also second only to HT2 samples. Under the wear load conditions, the soft RA is prone to deteriorated, which may lead to crack initiation caused by subsurface deformation, leading to plastic flow and delaminating (Ref 73). HT3 samples suffered less of crack formation due to lower austenite content. Therefore, compared with HT2 samples, extension cracks of HT3 samples were significantly increased, and boundary cracks appeared.

The frictional resistance is positively correlated with the number of cracks. In addition, the SNC are plowed out by friction pair material Si_3N_4 together with matrix material during wear. The EDS maps of the HT3 samples were exhibited in Fig. 10. In addition to chromium carbides, some silicon elements were also noticeable in the samples, indicating the potential presence of silicon material that may have peeled off from the friction pair. These SNCs can serve as rolling third bodies between Si_3N_4 and Cr12MoV matrices, which means that the sliding friction between the two mating surfaces changes to rolling friction, thereby reducing the weight loss and friction coefficient (Ref 54, 74, 75). The large number of SNC in HT3 samples reduces the friction resistance, making the weight loss and friction coefficient second only to HT2 samples.

The hardness of HT4 samples (688HB) is lower than that of HT3 samples with significantly higher RA volume fraction (9%) and slightly lower SNC than HT3 samples, resulting in the lower matrix hardness than HT3 samples. The high RA volume fraction further promoted the initiation of cracks in the matrix leading to lots of matrix cracks appeared in HT4 samples. Due to the low matrix strength, the cracks of primary carbides can extend to the matrix easily. Therefore, compared with HT3 samples, the number of extension cracks and boundary cracks in HT4 samples significantly increases, and carbide cracks disappeared. At the same time, the lower number of SNC compared with HT2 and HT3 samples result in the greatly increased friction resistance of HT4 samples, which is one of the reason for higher weight loss and friction coefficient of HT4 samples than that of HT3 samples.

The hardness of HT1 samples (677HB) is the lowest with highest RA volume fraction of the four samples and slightly more SNC than HT2 samples, leading to the lowest matrix hardness of the four samples. Therefore, the amount of matrix cracks in HT1 samples is higher than that in the HT4 samples. At the same time, the weight loss and friction coefficient of HT1 sample are the largest of the four samples.

Therefore, it can be inferred that the wear mechanism of Cr12MoV die steel is related to the hardness of the matrix structure, RA volume fraction and the amount of SNC. When the matrix hardness is high and the RA volume fraction is relatively low, the wear cracks are mainly carbide cracks and extension cracks, accompanied by a small number of boundary cracks. When the matrix hardness is low and the RA volume fraction is relatively high, the wear cracks are mainly matrix cracks, accompanied by some boundary cracks and extension cracks. DCT affects the wear mechanism of Cr12MoV die steel by facilitating the transformation of RA and the precipitation of SNC.
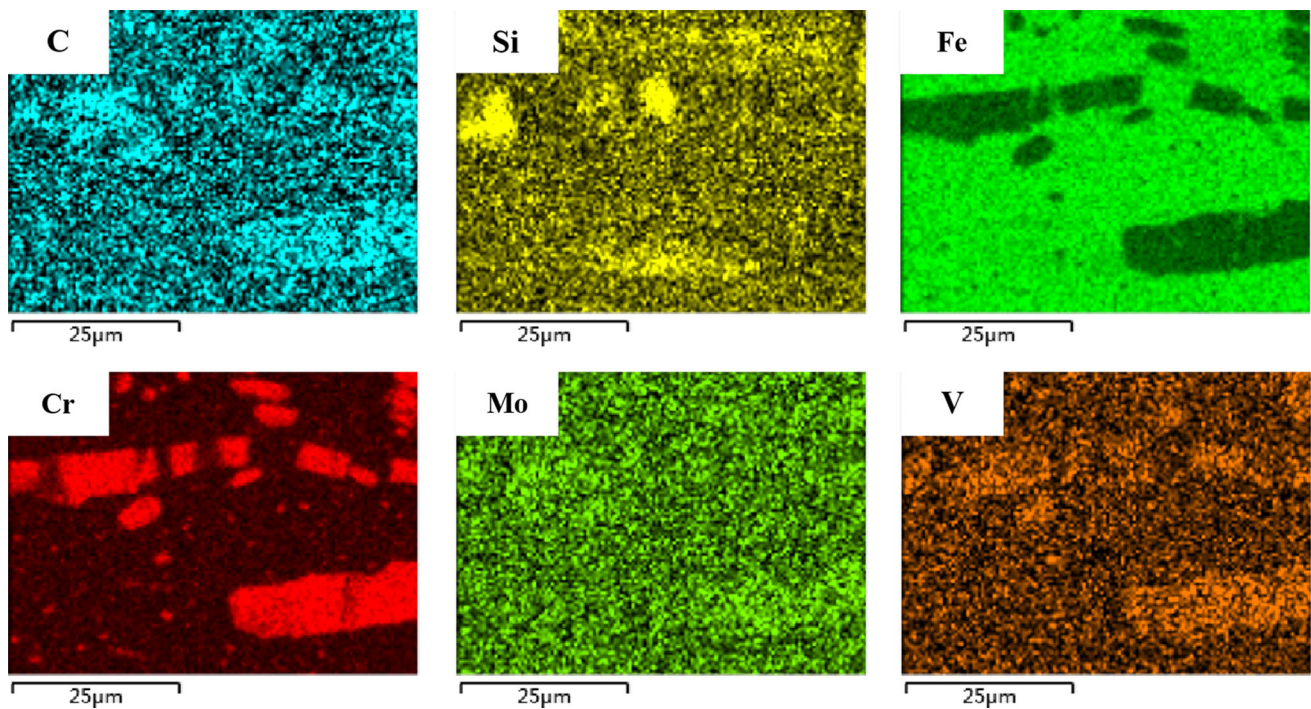
Fig. 10 EDS maps of HT3 sample

4. Conclusions

This research studied the microstructure evolution and wear resistance of Cr12MoV die steel during DCT. The following conclusions can be drawn:

1. DCT can contribute the transformation of RA into martensite and the precipitation of SNC from martensite, resulting in the improvement of hardness and wear resistance, and the reduction of toughness.
2. The method of DCT has an obvious influence on the microstructure of Cr12MoV die steel. Under the type of QCT, the lowest RA volume fraction was obtained, reaching 2%, which decreased by 84.6% compared with that of QT type. At the same time, the most homogeneous microstructure and the maximum amount of SNC was obtained under the type of QCT.
3. The method of DCT has an obvious effect on the mechanical properties of Cr12MoV die steel. Under the type of QC, the highest hardness was obtained, reaching 773HB, which was 14.2% higher than that of QT type. According to the weight loss, frictional coefficient and worn surface morphology results, the type of QC was recommended to achieve better wear resistance.
4. The precipitation of SNC has less effect on hardness than the reduction of carbon content in martensite that caused by DCT and tempering. The principal consideration for the high hardness and low toughness of the Cr12MoV die steel without tempering is the high carbon content in martensite. The RA volume fraction has greater effect on the hardness and toughness of the steel in condition of tempering.
5. Four types of wear cracks were observed in this study. When the matrix hardness is high and the RA volume fraction is relatively low, the wear cracks are mainly carbide cracks and extension cracks, accompanied by a small number of boundary cracks. When the matrix hardness is low and the RA volume fraction is relatively low, the wear cracks are mainly matrix cracks, accompanied by some boundary cracks and extension cracks. DCT affects the wear mechanism of Cr12MoV die steel by facilitating the transformation of RA and the precipitation of SNC.

References

1. D.N. Korade, K.V. Ramana, K.R. Jagtap and N.B. Dhokey, Effect of Deep Cryogenic Treatment on Tribological Behaviour of D2 Tool Steel—An Experimental Investigation, *Mater. Today Proc.*, 2017, **4**, p 7665–7673.
2. E. Macherauch, Ed, V. Hauk, Ed, Residual stresses in science and technology, Residual stresses in science and technology (1987)
3. S. Ren, Y. Zhang, Y. Zhao, Z. An, F. Xue, J. Yao, Z. Sun and J. Chang, Enhanced Surface Properties and Microstructure Evolution of Cr12MoV Using Ultrasonic Surface Rolling Process Combined with Deep Cryogenic Treatment, *J. Mater. Eng. Perform.*, 2019, **28**, p 1132–1140.
4. P. Baldissera, C. Delprete, Deep Cryogenic Treatment: A Bibliographic Review. The Open Mechanical Engineering Journal 2 (2008)
5. H. Li, W. Tong, J. Cui, H. Zhang, L. Chen and L. Zuo, The Influence of Deep Cryogenic Treatment on the Properties of High-Vanadium Alloy Steel, *Mater. Sci. Eng. A*, 2016, **662**, p 356–362.
6. P.V. Krot, S.V. Bobyr, N.V. Biba, and M.O. Dedik, Modeling of Phase Transformations in the Rolls of the Special Alloy Steels during Quenching and Deep Cryogenic Treatment. In *3rd Mediterranean Conference on Heat Treatment and Surface Engineering* (2016)
7. F.J.D. Silva, S.D. Franco, Á.R. Machado, E.O. Ezugwu and A.M. Souza Jr., Performance of Cryogenically Treated HSS Tools, *Wear*, 2006, **261**, p 674–685.

8. M.E. Mehtedi, P. Ricci, L. Drudi, S.E. Mohtadi, M. Cabibbo and S. Spigarelli, Analysis of the effect of Deep Cryogenic Treatment on the Hardness and Microstructure of X30 CrMoN 15 1 Steel, *Mater. Des.*, 2012, **33**, p 136–144.

9. S.S. Gill, J. Singh, R. Singh and H. Singh, Effect of Cryogenic Treatment on AISI M2 High Speed Steel: Metallurgical and Mechanical Characterization, *J. Mater. Eng. Perform.*, 2012, **21**, p 1320–1326.

10. A. Molinari, M. Pellizzari, S. Gialanella, G. Straffelini and K.H. Stiasny, Effect of Deep Cryogenic Treatment on the Mechanical Properties of Tool Steels, *J. Mater. Process. Technol.*, 2001, **118**, p 350–355.

11. D. Das, A.K. Dutta and K.K. Ray, Sub-Zero Treatments of AISI D2 Steel: Part I. Microstructure and hardness, *Mater. Sci. Eng. A*, 2010, **527**, p 2182–2193.

12. D. Das, A.K. Dutta and K.K. Ray, Sub-Zero Treatments of AISI D2 Steel: Part II. Wear Behavior, *Mater. Sci. Eng. A*, 2010, **527**, p 2194–2206.

13. A.K. Dutta, On the Refinement of Carbide Precipitates by Cryotreatment in AISI D2 Steel, *Philos. Mag.*, 2009, **89**, p 55–76.

14. A. Bensely, D. Senthilkumar, D.M. Lal, G. Nagarajan and A. Rajadurai, Effect of Cryogenic Treatment on Tensile Behavior of Case Carburized Steel-815M17, *Mater. Charact.*, 2007, **58**, p 485–491.

15. S. Zhirafar, A. Rezaeian and M. Pugh, Effect of Cryogenic Treatment on the Mechanical Properties of 4040 Steel, *J. Mater. Process Technol.*, 2007, **186**(1–3), p 298–303.

16. K. Sanjeev, S. Rakesh, and S. Vishal, Wear behavior of differently cryogenically treated AISI H13 steel against cold work steel, in *ARCHIVE Proceedings of the Institution of Mechanical Engineers Part E Journal of Process Mechanical Engineering 1989–1996* (2018) 095440891878162

17. M.J. Klug, P.J. Klug, T. Kranjec and B. Podgornik, Cross-effect of Surface Finishing and Deep Cryogenic Treatment on Corrosion Resistance of AISI M35 steel, *J. Mater. Res. Technol.*, 2021, **14**, p 2365–2381.

18. P. Jovievi-Klug, T. Kranjec, M. Jovievi-Klug, T. Kosec and B. Podgornik, Influence of the Deep Cryogenic Treatment on AISI 52100 and AISI D3 Steel's Corrosion Resistance, *Materials*, 2021, **14**, p 6357.

19. E. Bartolomé, B. Bozzo, P. Sevilla, O. Martínez-Pasarell and T. Puig, ABS 3D Printed Solutions for Cryogenic Applications, *Cryogenics*, 2017, **80**, p 32–37.

20. P. Jurči, M. Dománková, J. Ptačinová, M. Pašák, M. Kusý and P. Priknerová, Investigation of the Microstructural Changes and Hardness Variations of Sub-Zero Treated Cr-V Ledeburitic Tool Steel Due to the Tempering Treatment, *J. Mater. Eng. Perform.*, 2018, **27**, p 1514–1529.

21. P. Biswas, S. Ghosh, A. Sarkar and N.G. Roy, Investigation of Deep Cryogenic Treatment of Steels for Medical Tooling Applications, *J. Phys. Conf. Ser.*, 2021, **1797**, p 012057.

22. P. Jovievi-Klug and B. Podgornik, Review on the Effect of Deep Cryogenic Treatment of Metallic Materials in Automotive Applications, *Met Open Access Metall J*, 2020, **10**, p 434.

23. S. Kalia, Cryogenic Processing: A Study of Materials at Low Temperatures, *J. Low Temp. Phys.*, 2010, **158**, p 934–945.

24. M. Villa, and M.A.J. Somers, Cryogenic treatment of steel: from concept to metallurgical understanding, in *24th IFHTSE Congress 2017 European Conference on Heat Treatment and Surface Engineering A3TS Congress* (2017)

25. V.G. Gavriljuk, W. Theisen, V.V. Sirosh, E.V. Polshin, A. Kortmann, G.S. Mogilny, Y.N. Petrov and Y.V. Tarusin, Low-Temperature Martensitic Transformation in Tool Steels in Relation to Their Deep Cryogenic Treatment, *Acta Mater.*, 2013, **61**, p 1705–1715.

26. M.A. Jaswin and D.M. Lal, Effect of Cryogenic Treatment on Corrosion Resistance and Thermal Expansion of Valve Steels, *Int. J. Eng. Technol. Manag. Appl. Sci.*, 2015, **3**, p 2349–4476.

27. P. Jovičević-Klug, L. Tegg, M. Jovičević-Klug, R. Parmar, M. Amati, L. Gregoratti, L. Almásy, J.M. Cairney and B. Podgornik, Understanding Carbide Evolution and Surface Chemistry During Deep Cryogenic Treatment in High-Alloyed Ferrous Alloy, *Appl. Surf. Sci.*, 2023, **610**, p 155497.

28. P. Jovievi-Klug, M. Jovievi-Klug and B. Podgornik, Effectiveness of Deep Cryogenic Treatment on Carbide Precipitation, *J. Market. Res.*, 2020, **9**, p 13014–13026.

29. P. Jovičević-Klug, M. Jovičević-Klug, T. Sever, D. Feizpour and B. Podgornik, Impact of Steel Type, Composition and Heat Treatment Parameters on Effectiveness of Deep Cryogenic Treatment, *J. Mater. Res. Technol.*, 2021, **14**, p 1007–1020.

30. M. Villa and M.A.J. Somers, Cryogenic Treatment of an AISI D2 Steel: The Role of Isothermal Martensite Formation and "Martensite Conditioning," *Cryogenics*, 2020, **110**, p 103131.

31. P. Jovičević-Klug, M. Jenko, M. Jovičević-Klug, B.Š Batič, J. Kovač and B. Podgornik, Effect of Deep Cryogenic Treatment on Surface Chemistry and Microstructure of Selected High-Speed Steels, *Appl. Surf. Sci.*, 2021, **548**, p 149257.

32. J.Y. Huang, Y.T. Zhu, X.Z. Liao, I.J. Beyerlein, M.A. Bourke and T.E. Mitchell, Microstructure of Cryogenic Treated M2 Tool Steel, *Mater. Sci. Eng. A*, 2003, **339**, p 241–244.

33. P. Jovičević-Klug, M. Jovičević-Klug and B. Podgornik, Unravelling the Role of Nitrogen in Surface Chemistry and Oxidation Evolution of Deep Cryogenic Treated High-Alloyed Ferrous Alloy, *Coatings*, 2022, **12**, p 213.

34. K. Amini, S. Nategh and A. Shafyei, Influence of Different Cryotreatments on Tribological Behavior of 80CrMo12 5 Cold Work Tool Steel, *Mater. Des.*, 2010, **31**, p 4666–4675.

35. A.I. Tyshchenko, W. Theisen, A. Oppenkowski, S. Siebert, O.N. Razumov, A.P. Skoblik, V.A. Sirosh, Y.N. Petrov and V.G. Gavriljuk, Low-Temperature Martensitic Transformation and Deep Cryogenic Treatment of a Tool Steel, *Mater. Sci. Eng. A*, 2010, **527**, p 7027–7039.

36. S.M. Teus, V.F. Mazanko, J.M. Olive and V.G. Gavriljuk, Grain Boundary Migration of Substitutional and Interstitial Atoms in α-iron, *Acta Mater.*, 2014, **69**, p 105–113.

37. B.K. Anil Kumar, M.G. Ananthaprasad, and K. Gopalakrishna, Action of Cryogenic chill on Mechanical properties of Nickel alloy Metal Matrix Composites, In *Materials Science and Engineering Conference Series* pp. 012116 (2016)

38. V.G. Gavriljuk, W. Theisen, V.V. Sirosh, E.V. Polshin, A. Kortmann, G.S. Mogilny, Y.N. Petrov and Y.V. Tarusin, Low-temperature Martensitic Transformation in Tool Steels in Relation to Their Deep Cryogenic Treatment, *Acta Mater.*, 2013, **61**, p 1705–1715.

39. A. Antony, N.M. Schmerl, A. Sokolova, R. Mahjoub, D. Fabijanic and N.E. Stanford, Quantification of the Dislocation Density, Size, and Volume Fraction of Precipitates in Deep Cryogenically Treated Martensitic Steels, *Met. Open Access Metall. J.*, 2020, **10**, p 1561.

40. S. Akncolu, Investigation of the Effect of Deep Cryogenic Process on the Tribological Properties of X153CrMoV12 Mold Steel, *J. Mater. Eng. Perform.*, 2021, **30**, p 2843–2852.

41. R. Gecu, Combined Effects of Cryogenic Treatment and Tempering on Microstructural and Tribological Features of AISI H13 Steel, *Mater. Chem. Phys.*, 2022, **292**, p 126802.

42. L. Han, Y. Wang, S. Liu, Z. Zhang, X. Song, Y. Li, W. Liu, Z. Yang and M. Mu, Effect of Cryogenic Treatment on the Microstructure and Mechanical Properties of Selected Laser Melted H13 Steel, *J. Market. Res.*, 2022, **21**, p 5056–5065.

43. N.B. Dhokey, S.S. Maske and P. Ghosh, Effect of Tempering and Cryogenic Treatment on Wear and Mechanical Properties of Hot Work Tool Steel (H13), *Mater. Today Proc.*, 2021, **43**, p 3006–3013.

44. S. Katoch, R. Sehgal, V. Singh, M.K. Gupta, M. Mia and C.I. Pruncu, Improvement of Tribological Behavior of H-13 Steel by Optimizing the Cryogenic-Treatment Process Using Evolutionary Algorithms, *Tribol. Int.*, 2019, **140**, p 105895.

45. B.A. Mokarian, K. Ghayour and H. Gharavi, The Combined Effect of Cryogenic and Boronising Treatments on the Wear Behaviour and Microstructure of DIN 1.2344 Steel, *Trans. Inst. Met. Finish. Int. J. Surf. Eng. Coat.*, 2019, **97**, p 121–128.

46. M. Koneshlou, K.M. Asl and F. Khomamizadeh, Effect of Cryogenic Treatment on Microstructure, Mechanical and Wear Behaviors of AISI H13 Hot Work Tool Steel, *Cryogenics*, 2011, **51**, p 55–61.

47. E. Yildiz and S.Y. Tong, Investigation of the Effects of Deep Cryogenic Treatment on the Microstructure, Hardness, Strength and Wear Resistance of X17CrNi16-2 Martensitic Stainless Steel, *Surf. Rev. Lett.*, 2023, **30**, p 1–9.

48. R. Colaço and R. Vilar, Stabilisation of Retained Austenite in Laser Surface Melted Tool Steels, *Mater. Sci. Eng. A*, 2004, **385**, p 123–127.

49. M. Villa, K. Pantleon and M.A. Somers, Evolution of Compressive Strains in Retained Austenite During Sub-Zero Celsius Martensite Formation and Tempering, *Acta Mater.*, 2014, **65**, p 383–392.

50. A. Bensely, S. Venkatesh, D.M. Lal, G. Nagarajan, A. Rajadurai and K. Junik, Effect of Cryogenic Treatment on Distribution of Residual Stress

in Case Carburized En 353 Steel, *Mater. Sci. Eng. A*, 2008, **479**, p 229–235.

51. M. Preciado and M. Pellizzari, Influence of Deep Cryogenic Treatment on the Thermal Decomposition of Fe-C Martensite, *J. Mater. Sci.*, 2014, **49**, p 8183–8191.

52. S. Li, Y. Xie and X. Wu, Hardness and Toughness Investigations of Deep Cryogenic Treated Cold Work Die Steel, *Cryogenics*, 2010, **50**, p 89–92.

53. Z. Weng, K. Gu, J. Zheng, C. Cui, M. Zhang and J. Wang, Cryogenically Martensitic Transformation and Its Effects on Tempering Behaviors of Bearing Steel, *Mater. Charact.*, 2022, **190**, p 112066.

54. K. Amini, A. Akhbarizadeh and S. Javadpour, Effect of Deep Cryogenic Treatment on the Formation of Nano-Sized Carbides and the Wear Behavior of D2 Tool Steel, *Int. J. Miner. Metall. Mater.*, 2012, **19**, p 5.

55. P.F.D.S. Farina, C.A. Barbosa, and H. Goldenstein, Microstructural Characterization of an AISI D2 Tool Steel Submitted to Cryogenic Treatment, in 18th International IFHTSE Congress (2010)

56. D. Senthilkumar, I. Rajendran, M. Pellizzari and J. Siiriainen, Influence of Shallow and Deep Cryogenic Treatment on the Residual State of Stress of 4140 Steel, *J. Mater. Process. Technol.*, 2011, **211**, p 396–401.

57. K. Amini, A. Akhbarizadeh and S. Javadpour, Investigating the Effect of Holding Duration on the Microstructure of 1.2080 Tool Steel During the Deep Cryogenic Heat Treatment, *Vacuum*, 2012, **86**, p 1534–1540.

58. Y. Dong, X.P. Lin and H.S. Xiao, Deep Cryogenic Treatment of High-Speed Steel and Its Mechanism, *Heat Treat. Met.*, 1998, **25**, p 55–59.

59. F. Meng, K. Tagashira, R. Azuma and H. Sohma, Role of Eta-Carbide Precipitations in the Wear Resistance Improvements of Fe-12Cr-Mo-V-14C Tool Steel by Cryogenic Treatment, *Isij Int.*, 1994, **34**, p 205–210.

60. P. Jovicevic-Klug, M. Jovicevic-Klug, L. Thormahlen, J. Mccord, M. Rohwerder, M. Godec and B. Podgornik, Austenite Reversion Suppression with Deep Cryogenic Treatment: A Novel Pathway Towards 3rd Generation Advanced High-Strength Steels, *Mater. Sci. Eng. A Struct. Mater. Prop. Misrostruct. Process.*, 2023, **837**, p 145033.

61. S.S. Xu, Y. Zhao, D. Chen, L.W. Sun, L. Chen, X. Tong, C.T. Liu and Z.W. Zhang, Nanoscale Precipitation and Its Influence on Strengthening Mechanisms in an Ultra-High Strength Low-Carbon Steel, *Pergamon*, 2019, **13**, p 99–110.

62. O. Bouaziz and Y. Bréchet, Physical Relationship Between Mean-Field Micro-Mechanical Approach and Orowan Looping in Particle-Strengthened Materials, *Scr. Mater.*, 2009, **60**, p 366–368.

63. S. Jiang, H. Wang, Y. Wu, X. Liu, H. Chen, M. Yao, B. Gault, D. Ponge, D. Raabe, A. Hirata and M. Chen, Ultrastrong Steel Via Minimal Lattice Misfit and High-Density Nanoprecipitation, *Nature*, 2017, **544**, p 460–464.

64. Z.W. Zhang, C.T. Liu, Y.R. Wen, A. Hirata, S. Guo, G. Chen, M.W. Chen and B.A. Chin, Influence of Aging and Thermomechanical Treatments on the Mechanical Properties of a Nanocluster-Strengthened Ferritic Steel, *Metall. and Mater. Trans. A.*, 2012, **43**, p 351–359.

65. M. Hunkel, Tempering Effects of Athermal Martensite During Quenching and Reheating of a SAE 52100 Bearing Steel, *Mater. Sci. Eng. Struct. Mater. Prop. Misrostruct. Process.*, 2020, **790**, p 139.

66. D.N. Korade, K.V. Ramana and K.R. Jagtap, Study of Effect of Population Density of Carbides on Surface Roughness and Wear Rate of H21 Tool Steel – ScienceDirect, *Mater. Today Proc.*, 2019, **19**, p 228–232.

67. D. Kakas, B. Skoric, S. Mitrovic, M. Babic and M. Vilotic, Influence of Load and Sliding Speed on Friction Coefficient of IBAD Deposited TiN, *Tribol. Ind.*, 2009, **31**, p 3–10.

68. X.H. Cui, S.Q. Wang, M.X. Wei and Z.R. Yang, Wear Characteristics and Mechanisms of H13 Steel with Various Tempered Structures, *J. Mater. Eng. Perform.*, 2011, **19**, p 1055–1062.

69. S.J. Gobbi, V.J. Gobbi, G. Reinke, P.V. Muterlle and D.M. Rosa, Ultra-Low-Temperature Process Effects on Microscale Abrasion of Tool Steel AISI D2, *Mater. Sci. Technol.*, 2019, **35**, p 1355–1364.

70. S. Kumar, M. Nagraj, A. Bongale and N. Khedkar, Deep Cryogenic Treatment of AISI M2 Tool Steel and Optimisation of Its Wear Characteristics Using Taguchi's Approach, *Arab. J. Sci. Eng.*, 2018, **43**, p 4917–4929.

71. T. Shinde, C. Pruncu, N.B. Dhokey, A.C. Parau and A. Vladescu, Effect of Deep Cryogenic Treatment on Corrosion Behavior of AISI H13 Die Steel, *Materials*, 2021, **14**, p 7863.

72. R. Thakurai, H. Patle, B.R. Sunil and R. Dumpala, Effect of Cryogenic Treatment Duration on the Microhardness and Tribological Behavior of 40CrMoV5 Tool Steel, *Mater. Today Proc.*, 2020, **38**, p 2140–2144.

73. T. Shinde, Influence of Carbide Particle Size on the Wear Performance of Cryogenically Treated H13 Die Steel, *Surf. Eng.*, 2020, **37**, p 1206–1214.

74. Z. Jiang, L.A. Gyurova, A.K. Schlarb, K. Friedrich and Z. Zhang, Study on Friction and Wear Behavior of Polyphenylene Sulfide Composites Reinforced by Short Carbon Fibers and Sub-micro TiO_2 Particles, *Compos. Sci. Technol.*, 2008, **68**, p 734–742.

75. D. Felhs, J. Kargerkocsis, M.J. Churruca, P.M. Frontini and V. Pettarin, Changes in Tribological Performance of High Molecular Weight High Density Polyethylene Induced by the Addition of Molybdenum Disulphide Particles, *Wear*, 2010, **269**, p 31–45.